Electronic structure, vibrational properties, and optical spectra of two- and three-dimensional hexagonal InSe: Layer-dependent *ab initio* calculations

Mousa Bejani,[1] Olivia Pulci,[1] Naser Karimi,[2] Elena Cannuccia,[3] and Friedhelm Bechstedt[4]

[1]*Department of Physics, University of Rome, Tor Vergata, and INFN, Via della Ricerca Scientifica 1, I-00133 Rome, Italy*

[2]*Department of Science, Farhangian University, Tehran, 19989–63341, Iran*

[3]*Aix-Marseille Univ, PIIM, Laboratoire de Physique des Interactions Ioniques et Molculaires, UMR CNRS 7345, F-13397 Marseille, France*

[4]*Institut für Festkörpertheorie und -optik, Friedrich Schiller Universität, Max Wien Platz 1, D-07743 Jena, Germany*

(Received 8 February 2022; revised 4 August 2022; accepted 14 October 2022; published 7 November 2022)

We present a detailed study of the electronic properties and lattice dynamics of bulk and mono-, bi- and tri-tetralayer β-InSe by means of density functional and density functional perturbation theory. We show that the few-layers systems are semiconductors with an indirect nature of the fundamental band gap and a Mexican-hat-shape of the top valence band. The phonon branches analysis reveals the dynamical stability of a mono- and bi-tetralayer systems considered together with the longitudinal-optical–transverse-optical splitting breakdown toward one tetralayer. In-plane and out-of-plane zone-center lattice vibrations dominate the Raman and IR spectra. Small shifts of the peak positions but stronger variations of the peak intensities are observed as signatures of the number of layers.

DOI: 10.1103/PhysRevMaterials.6.115201

I. INTRODUCTION

Graphene [1–3] represents not only the most famous two-dimensional (2D) material, but also worked as a catalyst for the birth of a new field of 2D materials such as hexagonal boron nitride (h-BN) [4–6], transition metal dichalcogenides [7–10], and black phosphorus [11–13]. Scientists realized that layer-structured crystals bonded by van der Waals interaction are possible to be exfoliated into few and even a single layer, which may be deposited on top of suitable substrates [14,15]. In this respect, III-VI compound semiconductors represent an important group of layered van der Waals type materials, which are widely used as photodetecting materials [16] in photodetector [17–19] and photovoltage devices [20]. Moreover, they are used in well-known THz generators due to their large nonlinear effects [21,22].

InSe, as one of these III-VI semiconductors with extraordinary properties, has been taken into consideration in the last few years [23–25]. 2D few-layer InSe systems have been synthesized via physical [26–30] and chemical methods [24]. High tunability of the band gap with varying layer thickness has been confirmed by experimental and theoretical investigations [28–39]. Electronic band structures, vibrational, and optical properties and phonon behavior in single layers of InSe have been studied in recent years [31]. Also the structural and electronic properties of 2D bilayers of indium chalcogenides have been investigated [40].

Monolayer InSe consists of a Se-In-In-Se tetralayer (TL) covalently bonded in four atomic planes (see Fig. 1). Few-layer or bulk InSe systems are vertically stacked TLs, which are held together by a weak van der Waals (vdW) interaction [34]. Three highly distinct polytypes of the InSe crystal have been identified: β-InSe, γ-InSe, and ε-InSe [24,41,42], in which In and Se atoms, more precisely the TLs, are differently arranged. The γ polytype with ABCABC TL stacking (space group symmetry C^5_{3v}) is the most studied, showing a rhombohedral lattice [41,43]. Monolayer and few-layer γ-InSe stacks possess high electron mobility [26,44], excellent metal contact, and middle band gap range [44]. They offer the opportunity for favorizing tunable nanodevices. The β (ABAB stacking, space group symmetry D^4_{6h}) and ε polytypes (ACAC stacking, space group symmetry D^1_{3h}) are characterized by a hexagonal lattice consisting of eight atoms in the unit cell, which extends over two tetralayers [45]. β-InSe is the most stable phase of InSe [16]. The electronic band structures, work functions and optical properties of monolayer, few-layer, and bulk of β-stacking of InSe have been investigated and their layer thickness dependence has been demonstrated [25,38,39], also for similar compounds such as β-GaSe [46]. Although first theoretical investigations of the geometric configuration [47] and the electronic band structures [48–50] have been performed for monolayer systems, several studies on the layer-dependent valence band structure of InSe have also been carried out [38,39] to comprehend the tunable performances of the electronic and optoelectronic devices fabricated with different layer numbers. However, the details of the layer-dependent band structures and their consequences for optical emission, resonant tunneling spectroscopy, and spin-dependent transport are still under debate [51–54] In contrast to bulk and few-layer GaSe systems [46], the vibrational properties are less investigated [20,50,55]. This especially holds for the influence of the electron-phonon interaction on spectral and transport properties [56,57]. Theoretical studies of layer-dependent Raman and IR spectra are, to our knowledge, completely missing.

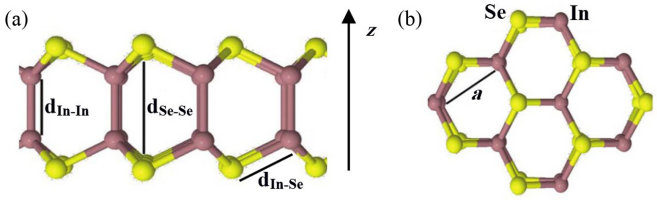

FIG. 1. (a) Side and (b) top view of the atomic geometry of an InSe tetralayer. The hexagonal in-plane lattice constant a, the thickness of a TL defined as the vertical distance $d_{Se\text{-}Se}$ between the top and bottom layer of selenium atoms in the normal z direction, the vertical In-In bond length $d_{In\text{-}In}$ and the In-Se bond length d_{In-Se} are also indicated.

In this work, we study 2D crystals and bulk of β-InSe in a systematic way. We calculate geometric configurations, electronic band structures, phonon branches, and Raman and IR spectra for different thicknesses (1TL, 2TL, 3TL and bulk) of β-InSe. In case of (dynamical) instability also other TL stackings are considered. The results are compared with available theoretical and experimental data on InSe. Also, consequences of the larger cation In in comparison to Ga are discussed. In a particular focus is the longitudinal-optical–transverse-optical (LO-TO) splitting breakdown in 2D systems [58], here illustrated for the mono- and few-layer InSe arrangements.

II. COMPUTATIONAL METHODS

The calculations of the geometric configurations and of the electronic properties are based on the density functional theory (DFT) [59] using different exchange-correlation (xc) functionals: the generalized gradient (GGA) approximation [60], proposed by Perdew, Burke, Ernzerhof (PBE) [61], and the local density approximation (LDA) [60], as implemented in the *ab initio* simulation QUANTUM ESPRESSO package (QE) code [62]. In the case of Indium, the semicore d electrons were included as valence electrons in the pseudopotentials. The weak vdW interaction between the tetralayers plays an important role in determining the interlayer distance between Se of different TLs in multilayer stacks as well as in bulk InSe. Consequently, for the bilayer (2TL), three-layer (3TL), and bulk β-InSe configurations, the vdW interaction was accounted for, by adding a semiempirical dispersion potential (D) to the conventional Kohn-Sham DFT energy [60], through a pairwise force field following Grimme's DFT-D2 method [63]. The electronic structures are not only described within PBE-vdW or LDA framework but also with inclusion quasiparticle correction in a simplified way: the screened-hybrid Heyd-Scuseria-Ernzerhof (HSE06) functional [64,65] was used to obtain the electronic band structures to compensate, at least partially, for the underestimation of the band gap by DFT [66].

For all layered structures of InSe, we performed the calculations using periodic boundary conditions and a vacuum space of about 16 Å between 1TL, 2TL, and 3TL in each supercell along the z direction, which is sufficient to bring the interaction among the periodic images to zero. The Monkhorst-Pack special k-point meshes [67] of $18 \times 18 \times 1$ are used to sample the Brillouin zone (BZ) of 1TL, 2TL, and 3TL, while $6 \times 6 \times 6$ is used for the bulk β-InSe for geometry optimization. All of the atomic structures were relaxed until forces were less than 10^{-8} a.u. The energy cutoff and convergence threshold are set to be 150 Ry and 1×10^{-16} Ry, respectively. For the phonon dispersion, Raman and IR spectra calculations, based on density functional perturbation theory (DFPT) [68], we use the LDA. Long-range interaction mediated by an in-plane electric field is taken into account [55,69]. A mesh of $9 \times 9 \times 3$ q points was used for the Raman and IR spectra of bulk, but $7 \times 7 \times 1$ for the 2D systems.

III. LATTICE STRUCTURES AND ELECTRONIC PROPERTIES

As a first step, we determined the equilibrium atomic geometry of InSe for bulk, three tetralayers (3TL), two tetralayers (2TL) and single tetralayer (1TL). The optimized lattice parameters are listed in Table I. In the 1TL case there is excellent agreement with other DFT-PBE calculations yielding $a = 4.05$ Å, $d_{Se\text{-}Se} = 5.39$ Å and $d_{In\text{-}In} = 2.287$ Å [47]. Other DFT studies [31] show excellent agreement for $d_{In\text{-}In}$ but some deviations for a and $d_{Se\text{-}Se}$ for both xc functionals, LDA and GGA + vdW.

The agreement between theory and experiment is also good. We found that the inclusion of the vdW interaction is important for the agreement with experiments in the case of multi-tetralayer structures. The bulk β-InSe lattice constants $a = 3.98$ Å and $c = 16.98$ Å in PBE + vdW compare well with the experimental values of $a = 4.05$ Å and $c = 16.93$ Å [25,39,70]. Our geometry-optimization calculations show that the PBE and LDA in-plane lattice parameter a decrease with increasing number of tetralayers from 1TL to bulk, like the In-In bond lengths, while the Se-Se distance increases from 1TL to bulk. The atomic distances obtained with the PBE functional are systematically larger than those optimized within the LDA, as expected [72]. The observed trends are similar to those found for GaSe [73]. These effects of the XC functionals as the chemical bonding strengths are also clearly visible in the total energies (E_{tot}) per TL in Table I.

Figure 2 displays the band structures in LDA quality of InSe upon reducing the number of layers from β-bulk to 3TL, 2TL, and 1TL. They clearly show the influence of intra-TL bonding, inter-TL interaction and symmetry on band position, splitting and dispersion. The number of bands follow the number of tetralayers in the unit cell. The chemical bonding within one tetralayer determines the band dispersion along the high-symmetry directions Γ-M-K- Γ rather independently of the number of TLs. The high symmetry of β-InSe with the space group $P6_3/mmc$ (D^4_{6h}) is expressed by the additional degeneracy of bands along the high-symmetry lines A-L-H-A in the top or bottom of the BZ. In contrast to the ε-polytype the band degeneracy is lifted [74]. This degeneracy has been also observed by other authors [38] and for β-GaS [75], β-GaSe [76], and lonsdaleite-Ge [77]. The group-IV crystal has the same symmetry. The interlayer interaction between two TLs in normal direction plays a minor role. This is clearly visible from the quite similarity of conduction bands along A-L-H-A lines for β-InSe and the Γ-M-K-Γ lines for 1TL.

TABLE I. Structural parameters of a TL in Å (as defined in Fig. 1), the distance $D_{\text{Se-Se}}$ between the most outermost Se atoms of two adjacent TLs (in Å), electronic indirect (E_g^{ind}) and direct band gaps (E_g^{dir}) (in eV) of 1TL, 2TL, 3TL and bulk. In addition, approximate quasiparticle direct gaps E_g^{HSE} (in eV) as derived from hybrid functional HSE06 calculations and using PBE + vdW lattice parameters are listed. The bulk hexagonal lattice constant c as well as the normalized total energy of the system (E_{tot}) (in eV/TL) are also given. The 1TL structure is used to define the energy zero. The DFT geometry calculations have been performed with the LDA and PBE + vdW exchange-correlation functional.

1TL	a	c	$d_{\text{In-In}}$	$d_{\text{Se-Se}}$	$d_{\text{In-Se}}$	$D_{\text{Se-Se}}$	E_g^{ind}	E_g^{dir}	E_{tot}	E_g^{HSE}
LDA	4.02	–	2.74	5.23	2.63	–	1.39	1.46	0	2.84
PBE(GGA)	4.09	–	2.83	5.37	2.69	–	1.34	1.43	0	
2TL										
LDA	3.97	–	2.74	5.28	2.62	3.73	0.99	1.08	−0.251	2.39
PBE(GGA) + vdW	4.05	–	2.80	5.37	2.67	3.76	0.98	1.04	−0.115	
3TL										
LDA	3.98	–	2.74	5.28	2.63	3.72	0.67	0.76	−0.367	1.98
PBE(GGA) + vdW	4.00	–	2.79	5.42	2.66	3.73	0.89	0.97	−0.237	
Bulk										
LDA	3.97	16.53	2.75	5.31	2.62	3.71	–	0.30	−0.415	1.84
PBE(GGA) + vdW	3.98	16.98	2.79	5.48	2.65	3.77	–	0.53	−0.324	
Exp [25,70]	4.05	16.93	2.78	5.48	2.68	3.82	–	–	–	1.26
Exp [71]	4.00		2.78	5.28	–	–	–	–	–	1.17

Valence bands tend to downshift in energy going from 1TL to the bulk case. The dispersion of the bands along the Γ-A direction can be identified as a rough measure of the strength of the interlayer interactions. The strong increase of the uppermost valence band along Γ-A makes the bulk a direct semiconductor, whereas the few-layer systems are indirect semiconductors.

The direct and indirect band gaps resulting from the band structure calculations (as displaced in Fig. 2) are also listed in Table I. The bulk compound shows a direct gap in PBE + vdW at the Γ point, which agrees with previous calculations [28–37]. With decreasing the number of tetralayers, as illustrated in Fig. 2, one can immediately see that a progressive confinement-induced shift leads to a direct gap at the Γ point increasing from the bulk value of 0.53 eV to about 1.43 eV for 1TL-InSe. Similar trends are visible for other xc functionals, LDA, and HSE06. In the LDA case the direct-gap variation goes from 0.3 to 1.46 eV. Similarly, the indirect gap with valence-band maximum somewhat out of the BZ center Γ varies from 0.85 (0.67) eV for 3TL to 1.34 (1.39) eV for 1TL within the PBE + vdW (LDA) framework. The HSE06 gaps are much larger and vary from 1.84 eV (bulk) to 2.84 eV (1TL). In the HSE06 case this increase is significant due to the inclusion of quasiparticle shifts in an approximate manner, through a fraction of exact (screened) exchange, of 1.0–1.4 eV (see Table I). Other HSE06 computations [31,39] give similar gap values, which, however, vary with the actually used numerical procedure and the inclusion of spin-orbit interaction (SOC). The SOC modification of the gap has been estimated to be about 0.12 eV for 1TL [36]. One

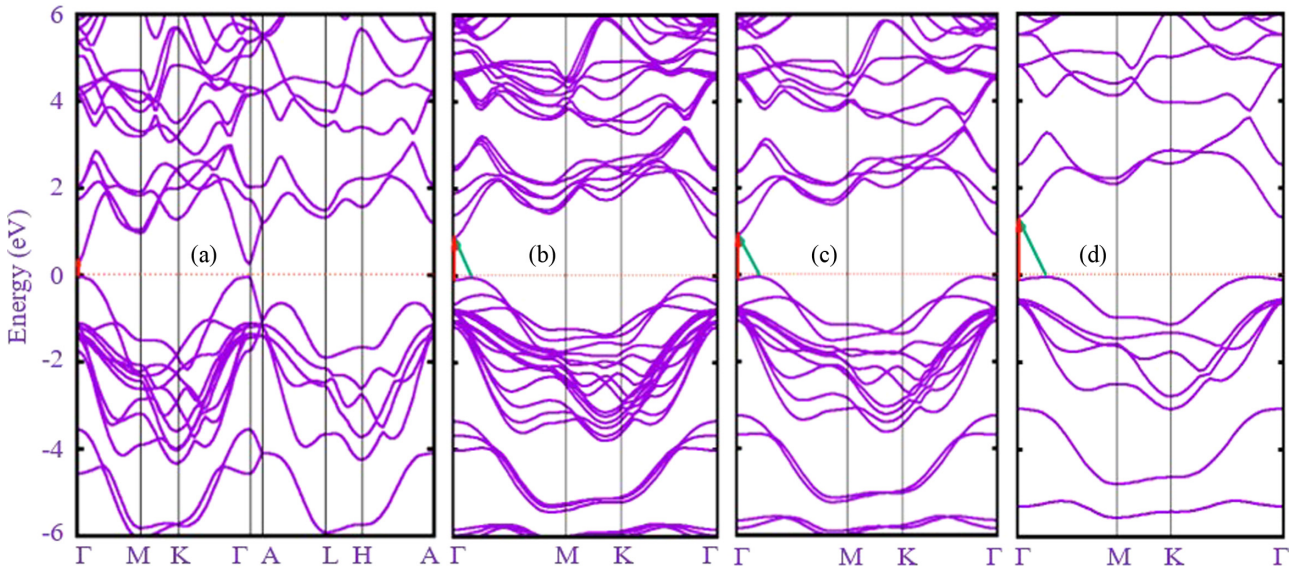

FIG. 2. Band structures of β-InSe, from (a) bulk to (b) 3TL, (c) 2TL, and (d) 1TL. The horizontal dotted lines display the valence band top as energy zero. The orange solid arrows indicate the direct band gaps, while the green solid arrows indicate the indirect band gaps.

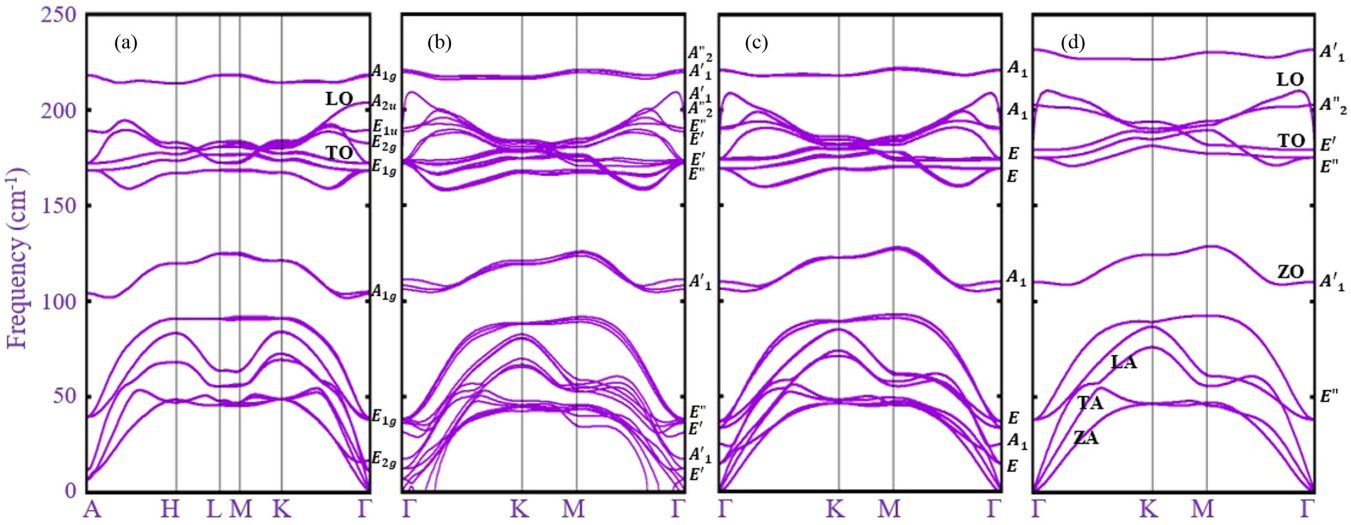

FIG. 3. Layer-dependent phonon dispersion curves of β-InSe from (a) bulk to (b) 3TL, (c) 2TL, and (d) 1TL determined using *ab initio* DFPT calculations.

has to take into consideration that the quasiparticle gap shift increases to about 2 eV for 1TL, if the more appropriate GW approximation is applied [48]. The 1TL gaps derived within DFT-PBE widely agree [47,78].

The InSe layered structures (see Fig. 2) exhibit a rather surprising crossover from a direct-gap to an indirect-gap semiconductor in the 2D sheet limit. These findings are in contrast to those for the well-studied MoS_2, [51,79] in which the indirect band gap in the bulk shifts upwards in energy by more than 0.6 eV with decreasing thickness, leading to another crossover from indirect- to direct-gap materials in the limit of the single monolayer, however, with a conduction-band minimum (CBM) outside Γ in the bulk band structure and the direct gap at K, a corner point of the 2D hexagonal BZ. Therefore, the band-symmetry characters of the direct-indirect crossover in InSe and MoS_2 are completely different and cannot be compared. In the β-InSe case the indirect character is mainly a consequence of Mexican-hat- or camel-back-like uppermost valence band. While the CBM appears at the Γ point in all layered InSe structures, independent of number of tetralayers, the position of the valence band maximum (VBM) varies with this number. The overall features of the calculated band structures for all configurations of 2D β-InSe sheets in Fig. 2 are quite consistent with each other, but also in qualitative agreement with the band behavior of GaSe [73]. When passing from 3TL to 1TL, the VBM shifts along the Γ–M and Γ–K lines. Since the CBM stays at the Γ point, indirect band gaps are obtained at all 2D tetralayer combinations. They get continuously enlarged significantly with decreasing number of TLs. Interestingly, the indirect gap in DFT-PBE in the 1TL-InSe case is only about 0.1 eV lower than the direct band gap. This energy difference also holds for 2TL and 3TL, although the absolute gap values are smaller. The valence band behavior will also influence the optical properties at the absorption edge. Theoretical predictions within the $\mathbf{k} \cdot \mathbf{p}$ theory and taking excitonic effects into account find the crossover between indirect and direct excitons in atomically thin films of InSe near 7 TLs [51].

IV. PHONON DISPERSIONS

Here, using the DFPT and the LDA xc-functional for LDA-optimized atomic equilibrium geometries, the dispersion of the phonon branches is plotted along the wave-vector path A-H-L-M-K-Γ (bulk) or Γ-K-M-Γ (layers) connecting high symmetry points in Fig. 3, from β-InSe, 3TL to 1TL. The phonon modes of bulk β-InSe can be categorized using the symmetry, i.e., the nonsymmorphic space group $D_{6h}{}^4$ and the point group D_{6h}. The symmetry has explicit consequences for the zone-center modes. The 24 Γ-modes of β-InSe with eight atoms extending over two TLs in a hexagonal unit cell can be decomposed according to their irreducible representations into $2(\mathrm{A_{2u}} \oplus \mathrm{E_{1u}} \oplus \mathrm{E_{2u}} \oplus \mathrm{A_{1g}} \oplus \mathrm{B_{1g}} \oplus \mathrm{B_{2u}} \oplus \mathrm{E_{1g}} \oplus \mathrm{E_{2g}})$ [42,76,80,81]. The $\mathrm{A_{2u}}$ and $\mathrm{E_{1u}}$ optical modes are infrared active, the $\mathrm{A_{1g}}$, E_{1g} and E_{2g} modes are Raman active, the $\mathrm{B_{1g}}$, $\mathrm{B_{2u}}$ and $\mathrm{E_{2u}}$ are neither infrared nor Raman active modes (optically inactive, silent modes). These normal modes are illustrated in Fig. 4. The three acoustic modes have A_{2u} or E_{1u} symmetry. The calculated bulk modes at Γ together with their symmetry character and the Raman and IR selection rules are shown in Table II. These results will be discussed below together with the Raman and IR spectra. Also, a comparison with experimental data is given. Indeed, the bulk Raman frequencies in Table II are in very good agreement with those of β-InSe measured for various temperatures (compare [42] and references therein).

As in the bulk case, for 1TL, 2TL, and 3TL systems Fig. 3 exhibits phonon branches with three acoustic modes of A or E symmetry. The E mode vibrating in-plane [longitudinal acoustic (LA) and transverse acoustic (TA)] is twofold degenerate at Γ and has a linear dispersion for vanishing wave vector. The A mode is a flexural phonon mode [out-of-plane acoustic mode (ZA)], which exhibits a peculiar quadratic dispersion near the zone center, typical of layered crystals [80] and can be explained as a consequence of the point group symmetry [25]. It is the easiest mode to be excited, because of its lowest frequency among all phonon modes and

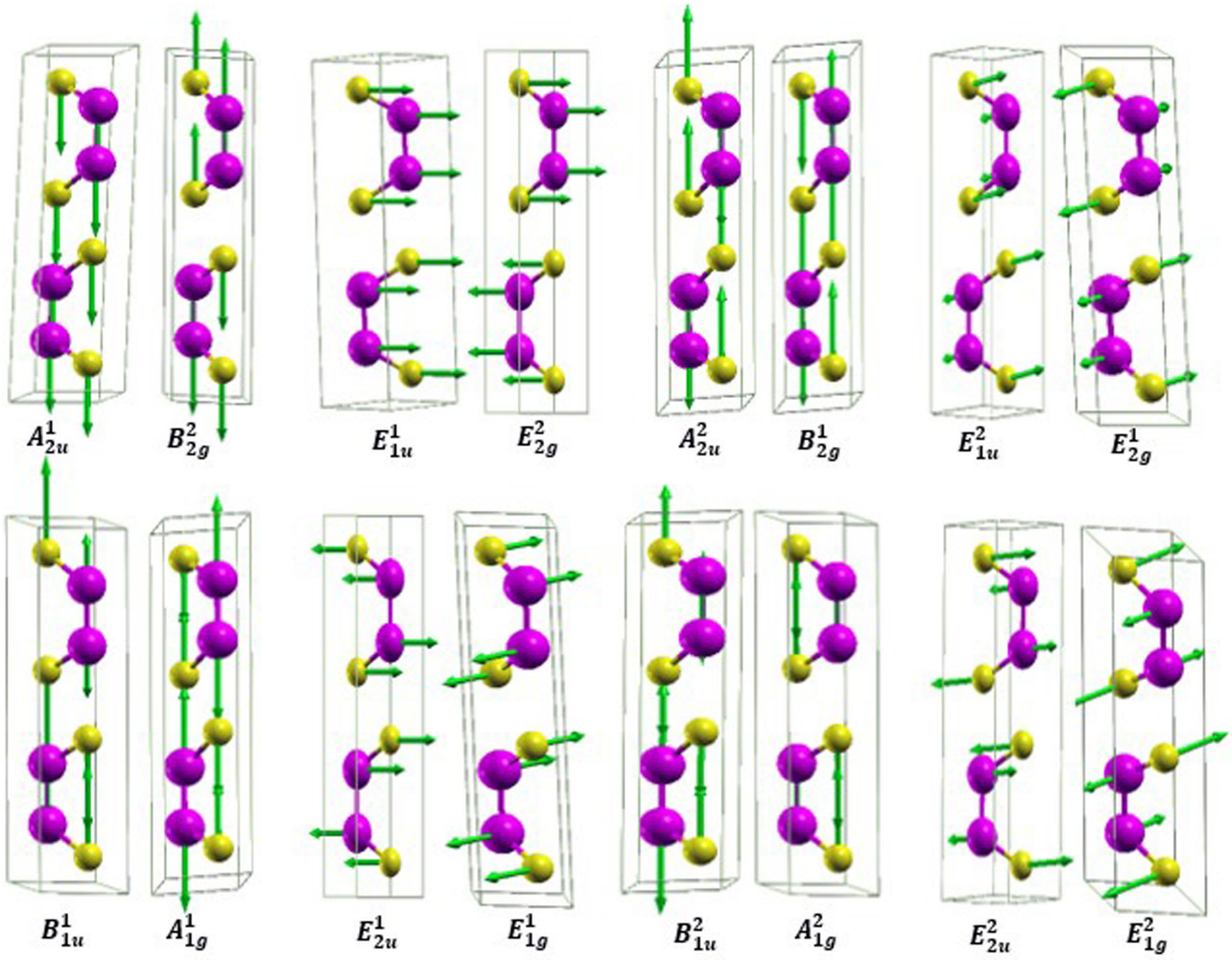

FIG. 4. In-plane (doubly degenerate E) and out-of-plane (A and B) normal modes of Γ phonons in bulk β-InSe illustrated by atomic displacements (green arrows) in the two TLs per unit cell. The bigger In (smaller Se) atoms are displayed as violet (yellow) balls. The modes are arranged in conjugate pairs.

it may be therefore easily affected by numerical instabilities [72]. In general, in the 1TL and 2TL cases the three acoustic branches converge smoothly to zero frequency for vanishing wave vector, demonstrating that numerical instabilities have been safely controlled. Moreover, no soft modes or negative energies appear in the phonon branches of bulk. We conclude that not only the bulk β-InSe but also the layered systems in β stacking are dynamically stable, at least, considering small 2D hexagonal unit cells.

In the 3TL nanosheets with β stacking, two of the acoustic modes have imaginary frequencies, thus suggesting that the layered 3TL β-stacked system is dynamically unstable. However, this result may be due to the difficulty in reaching accurate numerical convergence of the calculations because of the large supercells with 12 atoms and an appropriate amount of vacuum.

Such a tendency for a small pocket of instability has been observed earlier for mono-tetralayer InSe structures [31]. The authors found an extreme sensitivity to the details of the calculations. This fact has been interpreted as a general problem of phonon studies by means of first-principles calculations for 2D materials. It seems to indicate the general difficulty of achieving numerical convergence for the flexural phonon branches. Since in our study it only appears in the 3TL case, we studied the stacking effect more carefully. Beside the investigated β stacking, the ε- and γ-stacked 3TL systems also lead to minima on the total energy surface, i.e., to static stability within the LDA treatment. The LDA total energies of the three 3TL stackings compared to the mono-tetralayer 1TL are −0.367, −0.376 and −0.365 eV/TL for β, ε, and γ, respectively. These are close to each other as also observed for the bulk stacking [82,83]. The resulting ground-state parameters are also similar to the LDA values listed in Table I. This especially holds for the in-plane lattice constant a and the intra TL bond distances $d_{\mathbf{In\text{-}In}}$, $d_{\mathbf{Se\text{-}Se}}$, and $d_{\mathbf{In\text{–}Se}}$, which only weakly vary with the stacking. This finding is in agreement with the results for the β and ε stacking, i.e., the 2H polytype, and the γ stacking, i.e., the 3R polytype, in the bulk limit [82–84]. The phonon branches of 3TL in γ- and ε-stacking are displayed in Fig. 5. Despite the slightly reduced symmetry this figure shows similar phonon branches as the β stacking in Fig. 3(b). This essentially holds for the dispersion and the splitting of the phonon branches. The weak tendency for the negative frequency modes near Γ occurs for β, ε, and γ

TABLE II. Calculated Raman- and/or IR-active optical modes of β-InSe and 2D systems at zone center characterized by their irreducible representation, the frequency (in cm^{-1}), and Raman and IR intensities (in arbitrary units). The layer thickness varies between bulk, 3TL, 2TL, and 1TL. The irreducible representations of E and A character are also given. Slightly different denotations are given according to the point groups D_{6h} (bulk) and $D_{3h/d}$ (nanosheets). In the case of frequency splitting in the 2D case only the frequency which gives the highest spectral weight is listed.

Frequency (cm^{-1})								Raman Intensity (a.u.)				IR Intensity (a.u.)			
1TL		2TL		3TL		Bulk		1TL	2TL	3TL	Bulk	1TL	2TL	3TL	Bulk
		11.9	E	5.7	E''	17.0	E_{2g}	–	1.6	0.04	14.1				
				13.7	E'					5.8		–	0	0	0
		24.6	A_1	16.6	A'_1					0.15	0				
				30.4	A''_2	36.2	E_{2u}		0.1	0		–	0	0	0
39.0	E''	36.9	E	36.2	E''	36.5	B_{1g}	0.1	0	0.06	0	0	0	0	0
		38.6		37.3	E'	39.3	E_{1g}		3.5	2.8	479.6				
				38.6	E''					3.4					
110.2	A'_1	108.8	A_1	108.1	A'_1	107.9	B_{2u}	51.9	0	13.2	0				
		112.0		110	A''_2	114.5	A_{1g}		165.2	0	46163.8	0	0	0	0
				112.8	A'_1					273.6					
175.3	E''	174.3	E	173.4	E''	174.1	E_{1g}	0.2	2.5	3.5	3989.8	0	0.01	0	0
		174.3		173.5	E'	174.1	E_{2u}		4.8	5.1	0		0.0	0.02	0
				173.5	E''					4.8				0.01	
179.4	E'	178.3	E	177.3	E'	178.0	E_{2g}	0.9	0.2	6.8	12.9	5.5	9.2	6.2	11.2
		178.3		177.5	E''	178.0	E_{1u}		1.4	1.0	0		1.3	3.7	12.4
				177.5	E'					1.41				5.9	
202.8	A''_2	200.0	A_1	197.5	A''_2	190.7	A_{2u}	0	0	0	0	0.03	0.1	0.12	3.7
		200.5		198.7	A''_2	199.3	B_{1g}		25.4	0	0		0	0.06	0
				199.1	A'_1					32.4				0	
231.7	A'_1	229.4	A_1	227.1	A'_1	227.5	A_{1g}	161.8	391.8	397.2	647.1	0	0	0	0
		229.8		228.2	A'_1	228.5	B_{2u}		0.01	0.5	0				
				228.4	A''_2					210.5					

stacking but is only minor for the flexural branch. So, all three studied stackings seem to indicate some dynamical instability of the freestanding 3TL systems, although the tendency is very low for ε stacking. Because of the mentioned numerical problems, we, anyway, keep the β stacking to investigate the thickness dependence of Raman and IR frequencies and intensities in the following.

In the case of the three β-stacked multi-tetralayer 2D crystals considered, NTLs ($N = 1, 2, 3$), the space (point) group is somewhat reduced to $D^1{}_{3h}(D_{3h})$ for N odd and $D^3{}_{3d}$ (D_{3d}) for N even [81] with respect to bulk β-InSe with $D^4{}_{6h}(D_{6h})$. In the case of ε-stacked 3TL systems the $D^1{}_{3h}$ symmetry is conserved. As also indicated in Table II, Γ modes of bulk and NTL systems can be nearly related to each other. The bulk low-frequency breathing (out-of-plane) mode gives rise to (N-1) breathing A modes, while the bulk low-frequency shear mode appears as (N-1) doubly degenerated shear E modes in the 2D crystals [81]. Correspondingly, in Table II the Γ-modes of the NTL systems are grouped, in addition to the three acoustic modes, into eight categories, where bulk $E_{1g/u}$ and $E_{2g/u}$ modes appear as E modes in the few-tetralayer systems. The higher A_{1g} and A_{2u} are denoted without the index g or u in the tetralayer cases independent of number N. In the odd-numbered layer cases, 1TL to 3TL, for each representation the number of phonon modes reflects the number of tetralayers. The frequencies of the spectroscopically accessible optical modes are also listed in Table II together with the averaged Raman and IR intensities. From 1TL to 3TL the phonon frequencies only vary of few cm^{-1} because of the weak vdW bonding between tetralayers. The Γ modes of the 2TL system and bulk β-InSe have very similar properties such as their number, symmetry, frequency and IR or Raman activity.

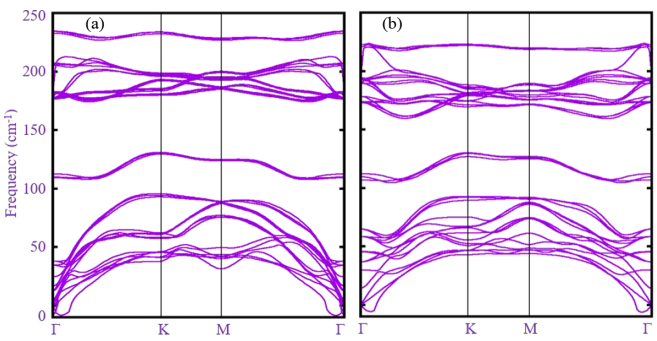

FIG. 5. Phonon branches of 3TL systems with γ (a) and ε (b) stacking.

Very interesting is the influence of the dynamical charge of ions on the optical phonon frequencies. For bulk InSe, more precisely the γ-polytype, it has been demonstrated by Raman measurements and model calculations that the long-range Coulomb interaction causes a LO-TO splitting near the Γ point [85,86]. We find such a LO-TO splitting near the Γ point of bulk, the TO mode is at about 174 cm^{-1} while the LO mode is above at about 200 cm^{-1}, as shown in Fig. 3(a) and Table II. In the isolated single tetralayer this splitting

vanishes. The frequencies of the two optical E modes merge at 179.4 cm^{-1} near the Γ point. The breakdown of the LO-TO splitting induces that in this limit the derivative of the LO phonon dispersion is discontinuous. Increasing the number of tetralayers the slope of the highest LO mode enlarges and the LO frequency smoothly approaches the bulk limit lifting the degeneracy [58]. In the 1TL case the vanishing LO-TO splitting has been also found by other authors [31,58]. A contradictory result has been however derived applying non-analytical corrections dominated by the dynamical charge to the dynamical matrix [55,69,87].

The long-range Coulomb interaction also plays an essential role in the structural stability of nanosheets of InSe [88], because without the long-range dipole-dipole interaction, the frequencies of acoustic modes become imaginary and the system is instable (not shown). Instead, when the long-range interaction is properly taken into consideration, the imaginary frequencies are eliminated and the 2D systems is dynamically stable. As shown in Fig. 3, apart from Fig. 3(b), we find no trace of imaginary frequencies in the Brillouin zone for bulk and small numbers of tetralayers. Therefore, the corresponding acoustic phonon dispersions suggest that isolated $N = 1, 2$ tetralayers and bulk of hexagonal β-InSe are dynamically stable.

The three lowest dispersion relations represent acoustic branches in each of the 1TL, 2TL, 3TL stacked systems and bulk. Other remnant branches are optical vibrations. 1TL, 2TL, 3TL and bulk have nine, 21, 33, and 21 optical branches, respectively. The irreducible representation associated with each phonon mode is labeled in Fig. 3. The lowest acoustic band has a quadratic behavior (labeled ZA in Fig. 3). It represents the flexural branch for out-of-plane vibrations and is therefore in-plane polarized. In Γ-K direction near Γ the dispersion relation $\omega \sim q^2$ with a fitting prefactor of 0.46×10^7 m^2s^{-1} is derived. Similar dispersion relations have been found elsewhere [87]. This quadratic behavior of the ZA band is a consequence of the fact that, at least to the lowest order in its amplitude, the strain energy created by this vibration is solely associated with the curvature that this out-of-plane bending mode induces in the layer. The other two acoustic branches are related to in-plane vibrations, a TA and a LA one, labeled in Fig. 3(d) in the low-frequency limit. The two linear branches have large sound velocities of ∼1526 m/s (TA) and ∼2696 m/s (LA) in the 1TL case. Other computations give rise to slightly larger velocities 1853, 1766 ms^{-1} for TA and 3398, 3272 ms^{-1} for LA [55,87] averaged over the ΓM and ΓK directions. In general, sound velocities of layered InSe are much lower than those of other 2D crystals, e.g., graphene or black phosphorene [89,90].

Immediately above the acoustic branches low-frequency optical modes are present in the bulk (17 cm^{-1}), 2TL (11.9 cm^{-1}) and 3TL (5.5−13.7 cm^{-1}). These modes are interlayer shear modes, typical for layered materials, corresponding to the sliding of two adjacent tetralayers. No shear modes are obviously present in the 1TL case. Above shear modes, optical bands typically converge much faster (including interactions with neighbors within the third or fourth nearest-neighbor shell). These E_{1g} or E modes have frequencies in a narrow interval between 36.2 and 39.3 cm^{-1}. According to the Raman and IR intensities in Table II they should be Raman active but IR forbidden. For 1TL our computed frequencies are only slightly larger than those in Ref. [31], where other numerical treatments were used. The variation of the next optical A_1 or A_{1g} modes with the number of TLs between 108.1 and 114.5 cm^{-1} is slightly more pronounced. As can be appreciated in Fig. 3 but also Table II, there is a separation between in-plane (in the range of 174.1 cm^{-1} in bulk to 179.4 cm^{-1} in 1TL) and out-of-plane modes (in the range of 190 cm^{-1} in bulk to 232 cm^{-1} in 1TL). This frequency separation is to be expected, since in-plane modes excite both bond stretching (hard) and bond-bending (soft), while out-of-plane modes result mostly in bond-bending motion and very little bond stretching. Another noteworthy characteristic of the phonon band structure displayed in Fig. 3 is the splitting of approximately 100 cm^{-1} existing between the ZO and ZA bands along M-K. In a homopolar hexagonal sheet such as graphene these two bands cross at K. The comparison with another 1TL calculations [31] indicates slightly higher frequencies for the upper optical phonons at Γ.

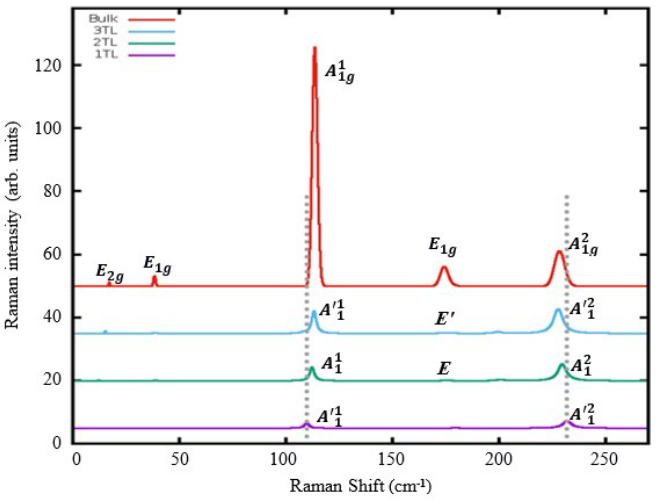

FIG. 6. Layer-dependent of Raman spectra of β-InSe bulk (red), 3TL (blue), 2TL (green), and 1TL (purple) determined using *ab initio* calculations.

V. RAMAN AND IR SPECTRA

The calculated Raman and IR spectrum for different numbers N of the TLs and β-InSe bulk are displayed in Figs. 6 and 7. The calculated dominant Raman and IR frequencies and their respective intensities as listed in Table II have been used for the construction of the spectra. The average of the frequencies weighted by the Raman intensities leads to the actual position of the Raman peaks in Fig. 6. Because of the geometrical similarities of the tetralayers and the weak vdW bonding between them, the corresponding vibrational frequencies of the longitudinal modes only vary with N by about 1–2 cm^{-1}. Due to the broadening applied, their narrow lines appear as one peak in the Raman spectra in Fig. 6. Independent of the number of tetralayers, two strong Raman peaks of A_{1g}/A_1 symmetry appear in the frequency range of 227–232 cm^{-1} and 110–114.5 cm^{-1}. The first (low

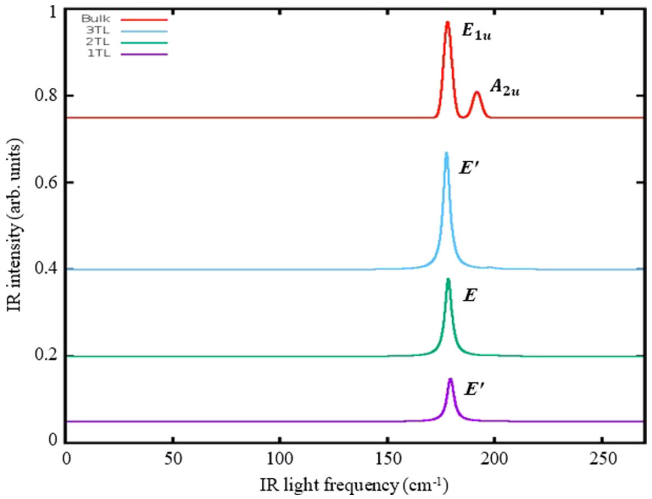

FIG. 7. Layer-dependent IR spectra of β-InSe bulk (red), 3TL (blue), 2TL (green), and 1TL (purple) determined using *ab initio* calculations.

frequency) ${A_{1g}}^1$ (${A_1}^1$) peak, corresponding to a stretching mode along z (see Table II), shifts toward lower frequencies by about 4 cm^{-1}. The high frequency ${A_{1g}}^2$ (${A_1}^2$) (see Table II) shifts by about 4 cm^{-1} to slightly higher energies with decreasing dimensionality. In the bulk case in-between another prominent Raman-active mode E_{1g} related to in-plane vibrations is visible. Weak Raman-active E_{1g} and E_{2g} modes may appear at much smaller frequencies (see also Table II). The strong out-of-plane vibrations of In-Se pairs, either of oppositely directed In and Se movements of the two pairs in one unit cell (${A_{1g}}^1$) or opposite displacements of In and Se atoms (${A_{1g}}^2$), also dominate the Raman spectra of the 1TL, 2TL and 3TL systems. The absolute peak position, with deviations of about 1–2 cm^{-1}, and the variations toward lower wave numbers with thickness of the lower ${A_{1g}}^1$ (${A_1}^1$) mode are in agreement with the experimental findings for hexagonal ε- and rhombohedral γ-InSe [24,29,91,92], where a mode near 200 cm^{-1} is present in the ε polytype but absent in the β polytype (see also Fig. 6) [42]. Indeed, the five-peak spectrum of bulk β-InSe is in excellent agreement with low- and room-temperature experimental findings [42] with maximum deviation of 3 cm^{-1} for the E_{1g} mode.

In the lower frequency range (in the first three rows in Table II) from the first up to the lower mode ${A_{1g}}^1$ (${A_1}^1$) one can see that the frequency decreases with vanishing material thickness, whereas in the high-frequency region the opposite behavior is observed for the last four rows up to mode ${A_{1g}}^2$ (${A_1}^2$) going from bulk InSe to 1TL. This opposite behavior found for the higher ${A_{1g}}^2$ (${A_1}^2$) mode, which shifts to higher wave numbers, is in agreement with experimental findings. However, the Raman peak in-between in the intermediate frequency range related to E (E_{1g}) modes does hardly vary with the material thickness, in agreement with the fact that they are in-plane modes. The ${A_{1g}}^1$ (${A_1}^1$) and ${A_{1g}}^2$ (${A_1}^2$) modes are out-of-plane vibrations and, therefore, more influenced by the thickness. Raman measurements on few-layer systems are rather rare [24,29,57,93]. A four TL system shows Raman modes at 114.5, 178.1, 202.1, and 227.3 cm^{-1} [93]. With more TL sheets similar frequencies have been measured but also one more peak near 212.4 cm^{-1} [29]. These findings are consistent with Raman studies on bulk γ crystals. For InSe flakes consisting of even more TLs three Raman modes at 117, 179, and 227 cm^{-1} have been found [24], indicating hexagonal stacking for which the mode around 200 cm^{-1} is missing (see also Fig. 6).

Similar to the GaSe case the IR spectrum of β-InSe in Fig. 7 is rather pure. Mainly E-derived peaks appear. In the bulk case, however, E_{1u} and A_{2u} modes are visible. Their excitation is related to dynamical dipoles in-plane (E_{1u}) or out-of-plane (A_{2u}). In the few-TL systems the out-of-plane mode disappears. Mainly the strong E_1 peak near 178 cm^{-1} survives down to 1TL. It only shifts by less than 2 cm^{-1} from bulk to 1TL in agreement with its in-plane character. In contrast to the data in Fig. 7, which result from an average over light polarizations, the experimental observation of the IR spectra depends on the angle of incidence and therefore requires a careful analysis in terms of ordinary and extraordinary light polarization.

VI. SUMMARY AND CONCLUSIONS

In this paper we investigated the atomic structure of 1TL, 2TL and 3TL β-InSe nanosheets by means of density functional theory. For comparison, the same calculations have been done for the bulk β-InSe crystal polytype. We studied three different exchange-correlation functionals in the ground-state calculations. We found the typical underestimation (overestimation) of the chemical bonding using – GGA- (LDA-) based functionals. We showed that the GGA + VdW functional delivers the bulk lattice constants in a sufficiently good agreement with measurements. The investigations of the electronic structures clearly indicated that the β-InSe nanosheets are indirect semiconductors because of a Mexican-hat dispersion of the uppermost valence band, while the bulk system is a direct semiconductor with the Γ-point position of both valence and conduction bands. Quasiparticle effects, in general, and confinement effects in the nanosheets increase the fundamental gaps toward values which are comparable with experimental data.

Phonon frequencies and dispersions together with resulting Raman and IR optical spectra have been calculated in the local-density framework applying the density functional perturbation theory. The lattice-vibrational properties are dominated by twofold degenerate in-plane E-type modes and nondegenerate out-of-plane A-type modes. The phonon band dispersion versus high-symmetry lines in the 2D hexagonal BZ shows that the few-tetralayer nanosheets are generally dynamically stable and that the phonon band dispersion of 1TL, 2TL, and 3TL exhibits the LO-TO splitting breakdown typical of polar two-dimensional systems. Only in the 3TL case do all the studied stackings β, γ, and ε show weak tendency for dynamical instability, which could originate from numerical reasons or could be cured by growing the sample on a substrate. The frequencies, Raman intensities, and IR oscillator strengths of the β stacking allow the construction of Raman and IR spectra in qualitative but also quantitative agreement with available experimental data. This holds for

the most intense peaks, in general, but also for the thickness dependence of their peak positions.

ACKNOWLEDGMENTS

Computational resources were granted by CINECA Marconi and ENEA CRESCO HPC centers. O.P. acknowledges financial funding from the EU MSCA-RISE project DiSeTCom (GA 823728) and from INFN (TIME2QUEST project). E.C. acknowledges the support of the French Agence Nationale de la Recherche (ANR) under reference ANR-20-CE47-0009-01 – NOTISPERF and is grateful for the support HPC resources from TGCC-CEA through Grant No. AD010913493.

[1] K. S. Novoselov, A. K. Geim, S. V. Morozov, D. Jiang, Y. Zhang, S. V. Dubonos, I. V. Grigorieva, and A. A. Firsov, Science **306**, 666 (2004).
[2] A. K. Geim and K. S. Novoselov, Nat. Mater. **6**, 183 (2007).
[3] J. C. Meyer, A. K. Geim, M. I. Katsnelson, K. S. Novoselov, T. J. Booth, and S. Roth, Nature (London) **446**, 60 (2007).
[4] G. Satta, G. Cappellini, M. Palummo, and G. Onida, Comput. Mater. Sci. **22**, 78 (2001).
[5] T. Ishii and T. Sato, J. Cryst. Growth **61**, 689 (1983).
[6] S. P. S. Arya and A. D'Amico, Thin Solid Films **157**, 267 (1988).
[7] B. Radisavljevic, A. Radenovic, J. Brivio, V. Giacometti, and A. Kis, Nat. Nanotechnol. **6**, 147 (2011).
[8] K. S. Novoselov, D. Jiang, F. Schedin, T. J. Booth, V. V. Khotkevich, S. V. Morozov, and A. K. Geim, Proc. Natl Acad. Sci. USA **102**, 10451 (2005).
[9] Y. Yoon, K. Ganapathi, and S. Salahuddin, Nano Lett. **11**, 3768 (2011).
[10] Y. Cai, G. Zhang, and Y.-W. Zhang, J. Am. Chem. Soc. **136**, 6269 (2014).
[11] L. Li, F. Yang, G. J. Ye, Z. Zhang, Z. Zhu, W. Lou, X. Zhou, L. Li, K. Watanabe, T. Taniguchi *et al.*, Nat. Nanotechnol. **11**, 593 (2016).
[12] J. Qiao, X. Kong, Z.-X. Hu, F. Yang, and W. Ji, Nat. Commun. **5**, 4475 (2014).
[13] Z.-X. Hu, X. Kong, J. Qiao, B. Normand, and W. Ji, Nanoscale **8**, 2740 (2016).
[14] E. Petroni, E. Lago, S. Bellani, D. W. Boukhvalov, A. Politano, B. Gürbulak, S. Duman, M. Prato, S. Gentiluomo, R. Oropesa-Nuñez *et al.*, Small **14**, 1800749 (2018).
[15] H. Cai, Y. Gu, Y.-C. Lin, Y. Yu, D. B. Geohegan, and K. Xiao, Appl. Phys. Rev. **6**, 041312 (2019).
[16] J. J. Wang, F. F. Cao, L. Jiang, Y. G. Guo, W. P. Hu, and L. J. Wan, J. Am. Chem. Soc. **131**, 15602 (2009).
[17] A. G. Kyazym-zade, A. A. Agaeva, V. M. Salmanov, and A. G. Mokhtari, Tech. Phys. **52**, 1611 (2007).
[18] C.-H. Ho, M.-H. Hsieh, and C.-C. Wu, Rev. Sci. Instrum. **77**, 113102 (2006).
[19] Z. D. Kovalyuk, O. A. Politanska, O. N. Sydor, and V. T. Maslyuk, Semiconductors **42**, 1292 (2008).
[20] J. F. Sánchez-Royo, A. Segura, O. Lang, C. Pettenkofer, W. Jaegermann, A. Chevy, and L. Roa, Thin Solid Films **307**, 283 (1997).
[21] S. A. Ku, W.-C. Chu, C. W. Luo, Y. M. Andreev, G. Lanskii, A. Shaidukoi, T. Izaak, V. Svetlichnyi, K. H. Wu, and T. Kobayashi, Opt. Express **20**, 5029 (2012).
[22] H. Dezaki, T. Tanabe, H. Y. Jin, and Y. Oyama, Key Eng. Mater. **500**, 58 (2012).
[23] S. R. Tamalampudi, Y. Y. Lu, U. R. Kumar, R. Sankar, C. D. Liao, B. K. Moorthy, C. H. Cheng, F. C. Chou, and Y. T. Chen, Nano Lett. **14**, 2800 (2014).
[24] S. Lei, L. Ge, S. Najmaei, A. George, R. Kappera, J. Lou, M. Chhowalla, H. Yamaguchi, G. Gupta, R. Vajtai *et al.*, ACS Nano **8**, 1263 (2014).
[25] W. Huang, L. Gan, H. Li, Y. Ma, and T. Zhai, CrystEngComm **18**, 3968 (2016).
[26] W. Feng, W. Zheng, W. Cao, and P. Hu, Adv. Mater. **26**, 6587 (2014).
[27] R. Beardsley, A. V. Akimov, J. D. G. Greener, G. W. Mudd, S. Sandeep, Z. R. Kudrynskyi, Z. D. Kovalyuk, A. Patanè, and A. J. Kent, Sci. Rep. **6**, 26970 (2016).
[28] M. Brotons-Gisbert, D. Andres-Penares, J. Suh, F. Hidalgo, R. Abargues, P. J. Rodríguez-Cantó, A. Segura, A. Cros, G. Tobias, E. Canadell *et al.*, Nano Lett. **16**, 3221 (2016).
[29] G. W. Mudd, S. A. Svatek, T. Ren, A. Patanè, O. Makarovsky, L. Eaves, P. H. Beton, Z. D. Kovalyuk, G. V. Lashkarev, Z. R. Kudrynskyi *et al.*, Adv. Mater. **25**, 5714 (2013).
[30] D. A. Bandurin, A. V. Tyurnina, G. L. Yu, A. Mishchenko, V. Zólyomi, S. V. Morozov, R. K. Kumar, R. V. Gorbachev, Z. R. Kudrynskyi, S. Pezzini *et al.*, Nat. Nanotechnol. **12**, 223 (2017).
[31] V. Zólyomi, N. D. Drummond, and V. I. Fal'ko, Phys. Rev. B **89**, 205416 (2014).
[32] D. Errandonea, A. Segura, F. J. Manjón, A. Chevy, E. Machado, G. Tobias, P. Ordejón, and E. Canadell, Phys. Rev. B **71**, 125206 (2005).
[33] P. Gomes da Costa, R. G. Dandrea, R. F. Wallis, and M. Balkanski, Phys. Rev. B **48**, 14135 (1993).
[34] J. F. Sánchez-Royo, G. Muñoz-Matutano, M. Brotons-Gisbert, J. P. Martínez-Pastor, A. Segura, A. Cantarero, R. Mata, J. Canet-Ferrer, G. Tobias, E. Canadell *et al.*, Nano Res. **7**, 1556 (2014).
[35] C. Sun, H. Xiang, B. Xu, Y. Xia, J. Yin, and Z. Liu, Appl. Phys. Express **9**, 035203 (2016).
[36] L. Debbichi, O. Eriksson, and S. Lebègue, J. Phys. Chem. Lett. **6**, 3098 (2015).
[37] Y. Sun, S. Luo, X.-G. Zhao, K. Biswas, S.-L. Li, and L. Zhang, Nanoscale **10**, 7991 (2018).
[38] A. V. Kosobutsky, Science Evolution **2**, 11 (2017).
[39] D. K. Sang, H. Wang, M. Qiu, R. Cao, Z. Guo, J. Zhao, Y. Li, Q. Xiao, D. Fan, and H. Zhang, Nanomaterials **9**, 82 (2019).
[40] T. Ayadi, L. Debbichi, M. Said, and S. Lebègue, J. Chem. Phys. **147**, 114701 (2017).
[41] G. Han, Z. G. Chen, J. Drennan, and J. Zou, Small. **10**, 2747 (2014).
[42] C. Carlone, S. Jandl, and H. R. Shanks, Phys. Status Solidi B **103**, 123 (1981).

[43] G. W. Mudd, A. Patanè, Z. R. Kudrynskyi, M. W. Fay, O. Makarovsky, L. Eaves, Z. D. Kovalyuk, V. Zólyomi, and V. Falko, Appl. Phys. Lett. **105**, 221909 (2014).

[44] K. Xu, L. Yin, Y. Huang, T. A. Shifa, J. Chu, F. Wang, R. Cheng, Z. Wang, and J. He, Nanoscale **8**, 16802 (2016).

[45] B. Gürbulak, M. Şata, S. Dogan, S. Duman, A. Ashkhasi, and E. F. Keskenler, Physica E **64**, 106 (2014).

[46] M. Rahaman, M. Bejani, G. Salvan, S. A. Lopez-Rivera, O. Pulci, F. Bechstedt, and D. R. T. Zahn, Semicond. Sci. Technol. **33**, 125008 (2018).

[47] W. Li and J. Li, Nano Res. **8**, 3796 (2015).

[48] H. L. Zhuang and R. G. Hennig, Chem. Mater. **25**, 3232 (2013).

[49] M. Zhou, R. Zhang, J. Sun, W.-K. Lou, D. Zhang, W. Yang, and K. Chang, Phys. Rev. B **96**, 155430 (2017).

[50] J. Liu, X. Yang, Z. Dai, Y. Zhao, and S. Meng, Eur. Phys. J. B **93**, 137 (2020).

[51] A. Ceferino, K. W. Song, S. J. Magorrian, V. Zólyomi, and V. I. Fal'ko, Phys. Rev. B **101**, 245432 (2020).

[52] J. Zultak, S. J. Magorrian, M. Koperski, A. Garner, M. J. Hamer, E. Tóvári, K. S. Novoselov, A. A. Zhukov, Y. Zou, N. R. Wilson *et al.*, Nat. Commun. **11**, 125 (2020).

[53] M. Zhou, D. Zhang, S. Yu, Z. Huang, Y. Chen, W. Yang, and K. Chang, Phys. Rev. B **99**, 155402 (2019).

[54] M. Zhou, S. Yu, W. Yang, W.-k. Lou, F. Cheng, D. Zhang, and K. Chang, Phys. Rev. B **100**, 245409 (2019).

[55] T. Pandey, D. S. Parker, and L. Lindsay, Nanotechnology **28**, 455706 (2017).

[56] A. V. Lugovskoi, M. I. Katsnelson, and A. N. Rudenko, Phys. Rev. Lett. **123**, 176401 (2019).

[57] M. Rahaman, M. A. Aslam, L. He, T. I. Madeira, and D. R. T. Zahn, Commun. Phys. **4**, 172 (2021).

[58] T. Sohier, M. Gibertini, M. Calandra, F. Mauri, and N. Marzari, Nano Lett. **17**, 3758 (2017).

[59] P. Hohenberg and W. Kohn, Phys. Rev. **136**, B864 (1964).

[60] W. Kohn and L. J. Sham, Phys. Rev. **140**, A1133 (1965).

[61] J. P. Perdew, K. Burke, and M. Ernzerhof, Phys. Rev. Lett. **77**, 3865 (1996).

[62] P. Giannozzi, O. Andreussi, T. Brumme, O. Bunau, M. Buongiorno Nardelli, M. Calandra, R. Car, C. Cavazzoni, D. Ceresoli, M. Cococcioni *et al.*, J. Phys. Condens. Matter **29**, 465901 (2017).

[63] S. Grimme, J. Antony, S. Ehrlich, and H. Krieg, J. Chem. Phys. **132**, 154104 (2010).

[64] J. Heyd, G. E. Scuseria, and M. Ernzerhof, J. Chem. Phys. **118**, 8207 (2003).

[65] J. Heyd, G. E. Scuseria, and M. Ernzerhof, J. Chem. Phys. **124**, 219906 (2006).

[66] F. Bechstedt, *Many-Body Approach to Electronic Excitations* (Springer, Berlin, 2015).

[67] H. J. Monkhorst and J. D. Pack, Phys. Rev. B **13**, 5188 (1976).

[68] S. Baroni, S. de Gironcoli, A. Dal Corso, and P. Giannozzi, Rev. Mod. Phys. **73**, 515 (2001).

[69] A. Shafique and Y.-H. Shin, Sci. Rep. **10**, 1093 (2020).

[70] L. I. Man, R. M. Imamov, and S. A. Semiletov, Kristallografiya in Russian **21**, 628 (1976).

[71] O. Madelung, Sov. Phys. Crystallogr. (English translation) 21, 355 (1976), *Semiconductors: Data Handbook Semiconductors: Data Handbook* (Springer, New York, 2004).

[72] F. Favot and A. Dal Corso, Phys. Rev. B **60**, 11427 (1999).

[73] M. Bejani, O. Pulci, J. Barvestani, A. S. Vala, F. Bechstedt, and E. Cannuccia, Phys. Rev. Mater. **3**, 124003 (2019).

[74] D. V. Rybkovskiy, N. R. Arutyunyan, A. S. Orekhov, I. A. Gromchenko, I. V. Vorobiev, A. V. Osadchy, E. Y. Salaev, T. K. Baykara, K. R. Allakhverdiev, and E. D. Obraztsova, Phys. Rev. B **84**, 085314 (2011).

[75] Y. Ma, Y. Dai, M. Guo, L. Yu, and B. Huang, Phys. Chem. Chem. Phys. **15**, 7098 (2013).

[76] M. K. Niranjan, Phys. Rev. B **103**, 195437 (2021).

[77] C. Rödl, J. Furthmüller, J. R. Suckert, V. Armuzza, F. Bechstedt, and S. Botti, Phys. Rev. Mater. **3**, 034602 (2019).

[78] S. Demirci, N. Avazlı, E. Durgun, and S. Cahangirov, Phys. Rev. B **95**, 115409 (2017).

[79] T. Cheiwchanchamnangij and W. R. L. Lambrecht, Phys. Rev. B **85**, 205302 (2012).

[80] S. Sucharitakul, N. J. Goble, U. R. Kumar, R. Sankar, Z. A. Bogorad, F.-C. Chou, Y.-T. Chen, and X. P. A. Gao, Nano Lett. **15**, 3815 (2015).

[81] R. Longuinhos and J. Ribeiro-Soares, Phys. Chem. Chem. Phys. **18**, 25401 (2016).

[82] J. Srour, M. Badawi, F. E. H. Hassan, and A. Postnikov, J. Chem. Phys. **149**, 054106 (2018).

[83] J. Srour, A. Postnikov, M. Badawi, and F. El Haj Hassan, Phys. Status Solidi B **254**, 1700120 (2017).

[84] L. d. Brucker, M. Moret, B. Gil, and W. Desrat, AIP Adv. **12**, 055308 (2022).

[85] C. Ulrich, M. A. Mroginski, A. R. Goñi, A. Cantarero, U. Schwarz, V. Muñoz, and K. Syassen, Phys. Stat. Sol. **198**, 121 (1996).

[86] M. Balkanski, P. G. Da Costa, and R. F. Wallis, Phys. Status Solidi **194**, 175 (1996).

[87] A. S. Nissimagoudar, J. Ma, Y. Chen, and W. Li, J. Phys.: Condens. Matter **29**, 335702 (2017).

[88] H. Zhou, Y. Cai, G. Zhang, and Y.-W. Zhang, Nanoscale **10**, 480 (2018).

[89] D. L. Nika, E. P. Pokatilov, A. S. Askerov, and A. A. Balandin, Phys. Rev. B **79**, 155413 (2009).

[90] A. Jain and A. J. H. McGaughey, Sci. Rep. **5**, 8501 (2015).

[91] S. Ashokan, K. P. Jain, M. Balkanski, and C. Julien, Phys. Rev. B **44**, 11133 (1991).

[92] T. Ikari, S. Shigetomi, and K. Hashimoto, Phys. Status Solidi **111**, 477 (1982).

[93] Z. Chen, J. Biscaras, and A. Shukla, Nanoscale **7**, 5981 (2015).